Catalysis Communications 119 (2019) 28–32

Contents lists available at ScienceDirect

Catalysis Communications

journal homepage: www.elsevier.com/locate/catcom

Short communication

# Selective styrene oxidation on alkaline tantalates $ATaO_3$ (A = Li, Na, K) as heterogeneous catalysts

Candelaria Leal Marchena[a,*], Gina A. Pecchi[b,c], Liliana B. Pierella[a]

[a] Centro de Investigación y Tecnología Química (CITeQ), UTN – CONICET, Maestro Marcelo López esq. Cruz Roja Argentina, 5016 Córdoba, Argentina
[b] Faculty of Chemical Sciences, Edmundo Larenas 129, University of Concepción, Chile
[c] Millenium Nuclei on Catalytic Processes Towards Sustainable Chemistry (CSC), Chile

ARTICLE INFO

*Keywords:*
Perovskite
Alkaline tantalates
Styrene
Benzaldehyde

ABSTRACT

A series of alkaline tantalates ($LiTaO_3$, $NaTaO_3$, $KTaO_3$) prepared using citrate method were characterized by powder X-ray diffraction, nitrogen adsorption isotherms, Fourier transform infrared spectroscopy, diffuse reflectance spectroscopy-UV–Vis and differential thermogravimetric analysis techniques and evaluated as heterogeneous catalysts in selective oxidation of styrene towards benzaldehyde. An increase in the catalytic activity was observed with the atomic radii of the alkaline cation, attributed to the detected crystalline perovskite structure and presence of segregated phases. The largest styrene conversion (58.4 mol%) and benzaldehyde selectivity (77 mol%) was obtained for $KTaO_3$ with no significant loss of activity after six catalytic reuses.

## 1. Introduction

Benzaldehyde is an organic aromatic aldehyde used principally as intermediate for industrial applications. Benzaldehyde can be commercially manufactured as a by-product of the catalytic oxidation of toluene to benzoic acid [1], by the hydrolysis of benzal chloride [2] and by photocatalytic conversion of benzyl alcohol [3] among others. These processes that use homogeneous catalysts at large temperature and pressure show rather poor benzaldehyde selectivity, in some cases with traces of chloride, not acceptable in pharmaceutical industries. Therefore, the selective oxidation of styrene is considerable interest in industrial processes [4,5], especially using cheaper and friendly environmentally oxidants such as hydrogen peroxide [6] as an alternative to the traditional inorganic oxidants such as $K_2Cr_2O_7$, $HNO_3$ and tert-butyl peroxide. Eventhough it has been reported different homogeneous catalysts for styrene oxidation [7,8], the difficulty of recovering the catalyst from the reaction medium is still a not resolved challenger, therefore the use of heterogeneous catalysts is an interested alternative. Additionally, the stability of the heterogeneous catalyst making possible the reusability of them is another feature highly desirable for industrial applications. For styrene oxidation, it has been reported large activity and selectivity towards benzaldehyde with transition metals modified zeolites heterogeneous catalysts such as $Co_3O_4$@HZSM-5, ZSM-11 and Y zeolites [9,10] and metal oxides, such as CaO, $Mg_{0.5}Cu_{0.5}Fe_2O_4$, $SrFe_2O_4$ [11,12] among other.

Perovskite type compounds ($ABO_3$) have been extensively studied as electronic and magnetic materials [13]. Recently, the generation of hydrogen by water splitting reactions [14] and photodegradation of organic compounds [15] on perovskites compounds has been also reported. Such number of catalytic oxidation applications has been attributed to their well-known properties of oxygen mobility and large stabilization of transition metals in not usual oxidation states within their structure [16]. The activity mechanism of perovskite type oxides is related to their corner shared $BO_6$ octahedron network that facilitate electron and oxygen transfer. Eventhough it has been reported that the A-site substitution by a different cation provides a high redox flexibility of the perovskite-type oxide [17], the effect of the nature of the A cation in the structural, textural and catalytic properties for oxidation reaction has not been extensively reported.

The aim of this work is to investigate the effect of the atomic radii in alkali tantalates $ATaO_3$ (A = Li, Na, K) to be used as heterogeneous catalysts in the selective oxidation of styrene towards benzaldehyde under mild reaction conditions. We report the synthesis, characterization and catalytic performance of purees and easily separable alkaline tantalates.

* Corresponding author.
*E-mail address:* cleal@frc.utn.edu.ar (C. Leal Marchena).

https://doi.org/10.1016/j.catcom.2018.10.016
Received 27 August 2018; Received in revised form 10 October 2018; Accepted 18 October 2018
Available online 19 October 2018
1566-7367/ © 2018 Published by Elsevier B.V.

## 2. Experimental

### 2.1. Preparation

Alkaline tantalates, $ATaO_3$ (A = Li, Na and K) were prepared by citrate method employing the corresponding alkaline acetates, hydrogen peroxide ($H_2O_2$) and citric acid. An aqueous dissolution of the alkaline acetate was mixed at room temperature with a stoichiometric amount of $TaCl_5$ previously dissolved in $H_2O_2$. Citric acid was added under constant stirring in a molar ratio of 3:1 to metal cation. The dissolution was further heated to 80 °C until a gel was formed followed by drying at 80 °C for 12 h and calcined at 700 °C for 10 h.

### 2.2. Characterization

The X-ray powder diffraction (XRD) patterns of the catalysts were obtained in a Rigaku diffractometer with Ni-filtered CuKα radiation (λ = 1.5418 Å). The standard scan parameters were 2°$min^{-1}$ for 2Θ from 20° to 90°. The phases were identified by comparing the diffraction patterns to the reference files in the EVA software. The nitrogen adsorption-desorption isotherms at 77 K were carried out for the Brunauer-Emmett-Teller (BET) specific surface area determination in a Tri Star II 3020 instrument. Fourier-transform IR spectra (FTIR) spectra were recorded in a Nicolet Magna-IR 550 instrument equipped with a quartz sample holder with KBr windows. Diffuse reflectance spectra (DRS-UV–vis) spectra were recorded using a UV–Vis JASCO V650 spectrophotometer with an integrating sphere and internal Spectralon coating. The thermal gravimetric analysis (TGA) measurements were carried out using a TG50 Shimadzu equipment under nitrogen with 15 mg of sample a heating rate of 10°C$min^{-1}$ in the temperature range 20–900 °C.

### 2.3. Catalytic evaluation

The catalytic oxidation of styrene (99.5%, Fluka) was carried out with $H_2O_2$ (30 wt%, Cicarelli) as oxidant agent in a glass flask reactor with magnetic stirring immersed in a thermostatized bath equipped with a reflux condenser. Each catalytic test was performed employing 100 mg of catalyst, 6 mL of acetonitrile (99.9%, Fluka) as solvent, a molar styrene/$H_2O_2$ ratio of 0.3 and a reaction temperature of 60 °C. The molar styrene/$H_2O_2$ ratio was chosen in order to have an excess of $H_2O_2$ favoring the styrene oxidation. Samples were periodically withdrawn filtered, analyzed and quantified by a Perkin Elmer GC Clarus 500 equipped with a FID detector and capillary column ZB-1. To complement the identification a mass spectrometry GC-Mass (Shimadzu QP 5050 GC-17 A) using a HP-5 capillary column was also employed. In order to evaluated the reusability of the catalysts, after a catalytic evaluation the catalyst was separated from the liquid phase, washed with acetonitrile, dried at 70 °C for 24 h and reused under the same experimental conditions.

## 3. Results and discussion

In order to confirm the formation of the perovskite structure and identify crystalline phases, in Fig. 1 is shown the XRD patterns of the alkaline tantalates. For $LiTaO_3$ a highly crystalline rhombohedral structure with hexagonal axis (JCPDS 71–0950) was obtained with absence of second phases and the XRD pattern of $NaTaO_3$, match with the one reported by Huang et al. [18] synthesized from sodium acetate precursor. The diffraction lines at 2Θ = 22.85°, 32.55°, 40.17°, 46.6°, 52.54°, 58°, 68.1°, 72.94° and 77.47° are attributed to orthorhombic perovskite-type structure (JCPDS 73–0878) and the smaller peaks at 2Θ = 29.7°, 36.48°, 38.68° and 50.98° are associated with $NaTa_3O_8$ (JCPDS 36–0441) as segregated phase. With regard to $KTaO_3$, the XRD diffraction pattern indicate a cubic structure (JCPDS 35–1036) with presence of $K_2Ta_2O_6$ (JCPDS 35–1464) as segregated phase. The small

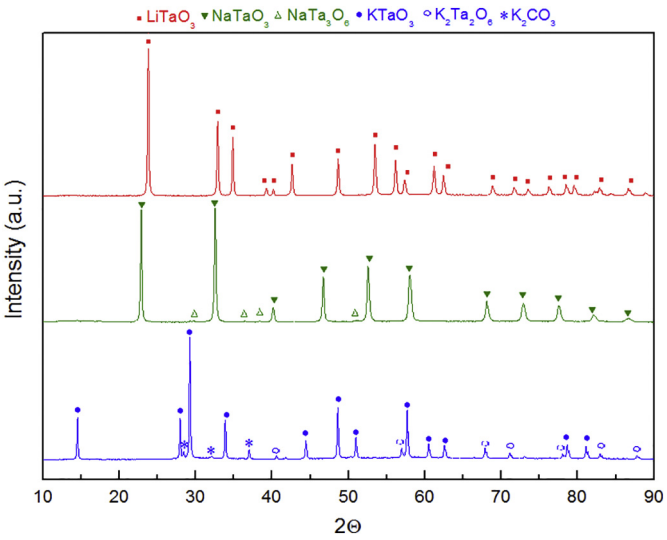


**Fig. 1.** XRD patterns of $LiTaO_3$, $NaTaO_3$ and $KTaO_3$.

peaks at 2Θ = 28°, 32° and 37.5° indicate presence of $K_2CO_3$ (JCPDS 42–1467) [19] in a lower extent.

Therefore, with the increases in the atomic radii of the alkaline cation, the diffraction patterns indicate an increase in the segregates phases and a decrease in the crystallinity [20]. From the Scherer's equation, the crystal size ($D_C$) for the perovskite structure was estimated and the results listed in Table 1. It can be seen an increase in the crystal size upon the increases of the ionic radii of the alkaline cation, this can be attribute to the change in the crystalline structure from rhombohedral to cubic [21]. The crystal size and structure of the perovskites are of great importance due to their strong structure-dependent physical properties [22].

In the FTIR spectra's of the alkaline tantalates shown in Fig. 2 it can be seen a broad band at 3300 $cm^{-1}$ associated to the O—H bond of water due to exposure to air and environmental humidity [23]. Additionally it is also present the main molecular absorption band of the perovskite structure at 610 $cm^{-1}$ assigned to the asymmetric stretching vibration for Ta—O bond and the stretching of longer bridging Ta–O–Ta bonds in the distorted $TaO_6$ octahedra [24]. The largest intensity and well defined band at 604 $cm^{-1}$ for $LiTaO_3$ is attributed to the symmetrical rhombohedral perovskite structure [21] and for $NaTaO_3$ the spectrum is quite similar to the reported by M. Yeh et al. [15]. In agreement with XRD results, the presence of carbonates as segregated phases only for $KTaO_3$ are also detected with the appearance of the bands at 1365 and 1402 $cm^{-1}$ associated to C—O bond [25].

The nitrogen adsorption isotherms at 77 K (Figure not shown) correspond to type II (IUPAC classification) characteristics of non-porous materials with almost no dependence with the alkaline cation. Lower specific surface areas values were obtained (Table 1), however not so different to the reported for perovskite-type structures [17]. The lower surface area of the $LiTaO_3$ can be correlated to the larger crystallinity of the structure.

The DRS-UV–Vis spectra's were carried out to evaluate the coordination geometry and chemical arrangement of the Ta species. In

**Table 1**
BET surface area, crystal size, band-gap, global pseudo first order constant and initial reaction rate of alkaline tantalates.

| Catalyst | $S_{BET}$ ($m^2/g$) | $D_C$ (nm)[a] | Eg (eV) | k ($h^{-1}$) | $r_0$ ($mmol g^{-1} h^{-1}$) |
|---|---|---|---|---|---|
| $LiTaO_3$ | 4 | 7.8 | 4.5 | 0.06 | 5.4 |
| $NaTaO_3$ | 7 | 8.0 | 4.1 | 0.15 | 13.6 |
| $KTaO_3$ | 8 | 8.9 | 3.3 | 0.26 | 23.0 |

[a] Estimated by Scherrer's equation.

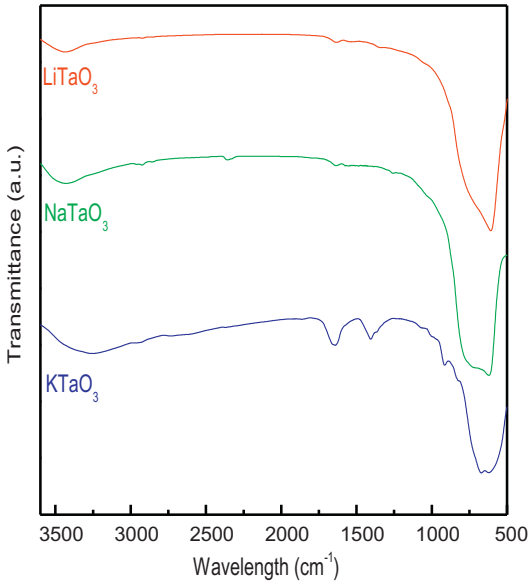


**Fig. 2.** FTIR spectra of $LiTaO_3$, $NaTaO_3$ and $KTaO_3$.

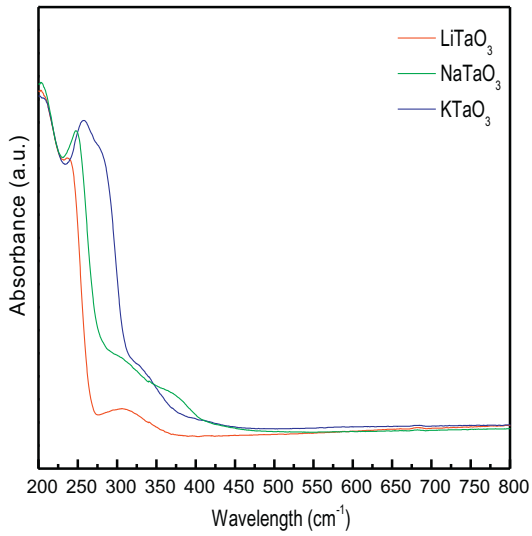


**Fig. 3.** DRS UV–Vis spectra of $LiTaO_3$, $NaTaO_3$ and $KTaO_3$.

Fig. 3 is seen a similar spectra for the alkaline tantalates with some differences in the maximum of the absorbance bands, attributed to the Ta-O-Ta bond. The bands at 240 nm ($LiTaO_3$), 249 nm ($NaTaO_3$), 280 nm ($KTaO_3$) and a lower intensity band of $NaTaO_3$ at 310 nm appears at lower wavelength that the corresponding $KTaO_3$ structure (328 nm). The shifts towards large wavelengths can be correlated with the Ta–O–Ta angles of their respective crystalline structure. In the rhombohedral structure of $LiTaO_3$ the Ta-O-Ta bond form angles of 143°, 163° in the orthorhombic structure of $NaTaO_3$ [15] and 180° in the more symmetric cubic $KTaO_3$ structure, in line with previous report [26].

The band gap energy values (Eg) were estimated from DRS-UV–Vis spectra using Kubelka–Munk remission function. The corresponding Eg values between the valence and conduction bands of O 2*p* and Ta 5*d* [18] are shown in Table 1. The observed values are similar to previously reported values [20] and show a decrease upon the ionic radii of the alkaline metal. This can be attributed due to the distortion of the crystalline structure as a consequence of the connection between the $TaO_6$ octahedra.

Thermal gravimetric analysis (TGA) of the alkaline tantalates were carried out up to 900 °C. The resulted profiles are in line with the previous discussion of FTIR and XRD techniques. The first weight loss at ($T$ > 150 °C) assigned to the elimination of free and bound water and the removal of organic compounds is lower than 1% for $LiTaO_3$ and $NaTaO_3$ and 2% for $KTaO_3$. The second weight loss around 250 °C assigned to the decomposition of residual organic groups [27] as carboxylates is detected only in $KTaO_3$ and at temperatures larger than 400 °C a slight (< 2%) weight loss for $NaTaO_3$ and $KTaO_3$ indicates presence of segregated species also detected by XRD. The shape and total weight loss (< 5%) confirm the previous characterization results.

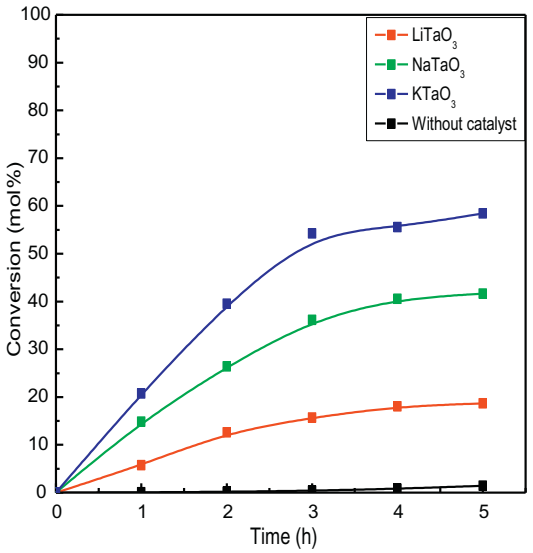


**Fig. 4.** Catalytic activity as a function of reaction time. *Reaction parameters:* styrene 9 mmol; $H_2O_2$ 30 mmol; solvent acetonitrile; catalyst amount 100 mg; temperature 60 °C; reaction time 5 h.

The experimental styrene conversion level upon reaction time is displayed in Fig. 4. It is also informed the non-catalytic reaction with almost no conversion up to 5 h of reaction (1.4%mol). In line with previous results [28,29], a dependence of the catalytic activity with the increase of the atomic number of the A-cation (K > Na > Li) is also detected. The catalytic performance in oxidation reactions for perovskite type oxides has been correlated to their surface area, surface electron density that promote electron transfer and crystalline structure [20,28]. Due to the largest crystallinity of the perovskite structure decreases the oxygen mobility [30], for catalytic oxidation applications it is desirable large extent of weakly binding surface oxygen.

It was found that with the increase of the atomic radius of A-cation, the crystallinity of the tantalates decrease, the oxygen mobility increases with not a large modification of the surface area. Hence, the different catalytic performance of $NaTaO_3$ and $KTaO_3$, with similar surface area and crystal size display should be attributed to their structural differences. In this way, Marchelek et al. [26] report lower catalytic performance in toluene degradation for octahedral $KTaO_3$ compared to the cubic structure. This has been attributed to rotations of the oxygen octahedra that has important impact on crystal structure and changes the dipole and electronic band structures. These changes influence the behaviors of the catalysts in redox reaction [31]. Moreover, the lowest crystallinity degree of $KTaO_3$ allows the easier oxygen mobility, essential for oxidation reactions. Additionally, $KTaO_3$ present the larger number of segregated phases which contributes to the larger catalytic activity, in particular $K_2CO_3$ [32]. With regard to $LiTaO_3$, the lower value of surface area, the possibility of the consequent agglomeration and the lower oxygen mobility associated to the higher crystallinity could be the contribution for their low catalytic performance [15,30]. The initial reaction rate ($r_0$) and global pseudo first order constant (k) calculated from the fit of the experimental data to a pseudo

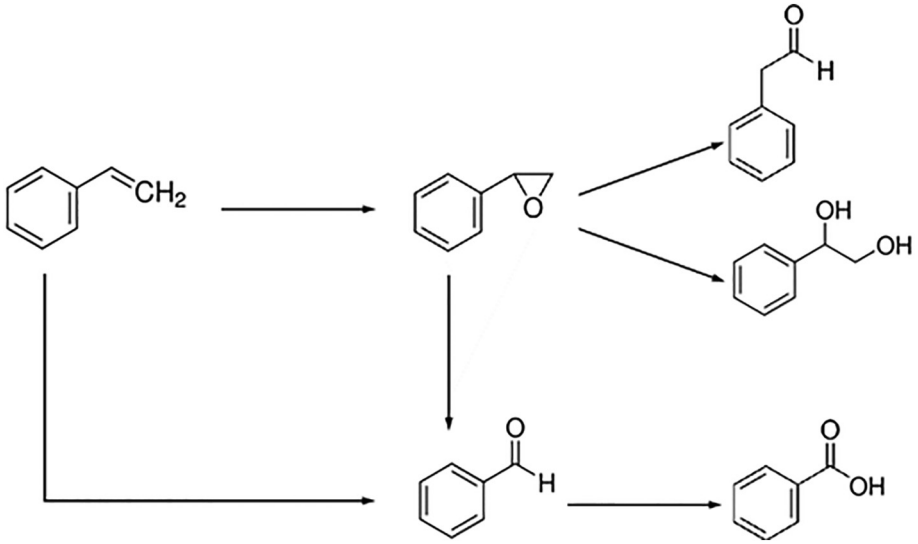


**Scheme 1.** Proposed scheme of styrene oxidation reaction.

first order are listed in Table 1. The correlation coefficient larger than 0.98 in all cases support the increases of k and $r_0$ with the atomic A cation radii.

The large benzaldehyde selectivity (> 73 mol%) of the alkaline tantalates and formation of styrene oxide as principal secondary product and phenylacetaldehyde, 1-phenylethane-1,2diol, benzoic acid in a lower extent as other secondary products is in agreement with Pierella et al. [33] reaction products. The oxidation of styrene by two different pathways is proposed in Scheme 1. For one hand, by an epoxidation reaction, styrene can form styrene oxide followed by a nucleophilic attacked to benzaldehyde and/or others secondary products. Another pathway is by a radical mechanism from the direct oxidative cleavage of the C=C bond of styrene by hydroxyl radicals formed from the surface decomposition of a molecule of $H_2O_2$.

Therefore, the obtained amount of benzaldehyde can be formed by the consecutive oxidation of styrene oxide and/or by direct oxidative cleavage of styrene. Moreover, in line with styrene oxidation reports [34], the slight increases of benzaldehyde selectivity with the ionic radii of the A cation, could be the attributed to the promotion of mass transfer in the reaction medium by the polarity of the solvent.

Due to benzaldehyde can be further oxidized to benzoic acid [35], in order to confirm the coexistence of these two pathways, a radical scanvenger (potassium iodide) was added after 1 h of reaction to the $KTaO_3$ catalytic reaction medium. It was found that in this reaction condition, styrene conversion decrease from 58.4 to ~20 mol%, indicative that the oxidation with the alkaline tantalates follows both reaction mechanism.

Due to the reusability of the catalyst is an attractive benefit of heterogeneous catalysis, the catalyst with the largest catalytic performance ($KTaO_3$) was selected in order to evaluate the reuses described in the catalytic evaluation section. In Fig. 5 is shown the styrene conversion and benzaldehyde, epoxide and other secondary products selectivity after six reuse cycles. The slight decreases in the catalytic behavior confirm the stability and recyclable application of the catalyst. The unavoidable loss of catalyst during filtration [35] and/or leaching of some species not embedded in the crystalline structure due the large dielectric constant of the solvent can be present in the studied recycles.

## 4. Conclusions

Alkaline tantalates were prepared, characterized and used as heterogeneous catalysts in the styrene oxidation. It was found an increases in the styrene conversion upon the ionic radii of the A-cation from

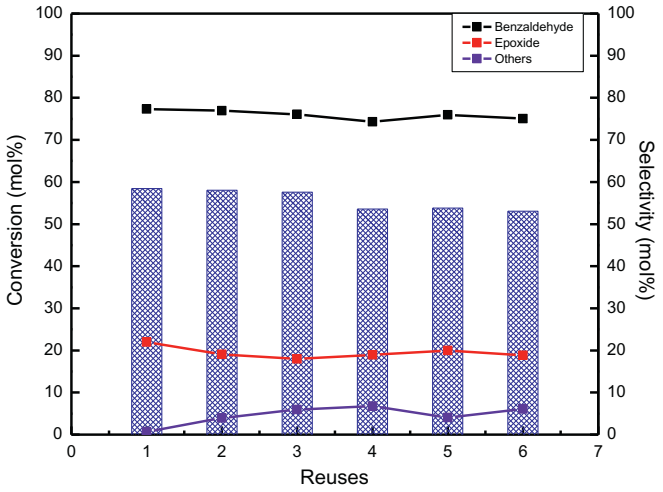


**Fig. 5.** Conversion and selectivity (%mol) of reused $KTaO_3$. *Reaction parameters:* styrene 9 mmol; $H_2O_2$ 30 mmol; solvent acetonitrile; catalyst amount 100 mg; temperature 60 °C; reaction time 5 h.

$LiTaO_3$ (18.7 mol%), $NaTaO_3$ (41.6 mol%) up to $KTaO_3$ (58.4 mol%) with almost no differences in the benzaldehyde selectivity as mayor secondary product. The largest catalytic activity of $KTaO_3$ can be attributed to the lower crystallinity associated to large mobility of the lattice oxygen essential for oxidation reactions, larger surface area and presence of carbonate potassium as segregated phases. $KTaO_3$ was successfully used as an attractive heterogeneous, reusable and recyclable catalyst for at least six consecutives reuse cycles with no thermal regeneration. This result indicates the potential use of alkaline tantalates as catalysts for oxidations under mild reaction conditions and point out the importance of the perovskite structure, associated with crystalline structure, segregated phases and oxygen mobility, in the catalytic oxidation reaction.

## Acknowledgments

Leal Marchena and Pierella thank financial support from CONICET and UTN. Pecchi FONDECYT 1170083 and Funding from Millennium Science Initiative of the Ministry of Economy, Development and Tourism, grant Nuclei on Catalytic Processes towards Sustainable Chemistry *(NM-CSC)*.

## References


[1] Y. Zhu, H. Wang, B. Wang, X. Liu, H. Wu, S. Licht, Solar thermoelectric field plus photocatalysis for efficient organic synthesis exemplified by toluene to benzoic acid, Appl. Catal. B Environ. 193 (2016) 151–159.

[2] G.D. Yadar, B.V. Haldavanekar, Mechanistic and kinetic investigation of liquid – liquid phase transfer catalyzed oxidation of benzyl chloride to benzaldehyde, J. Phys. Chem. A 101 (1997) 36–48.

[3] M. Lima, A. Silva, C. Silva, J. Faria, Graphitic carbon nitride modified by thermal, chemical and mechanical processes as metal-free photocatalyst for the selective synthesis of benzaldehyde from benzyl alcohol, J. Catal. 353 (2017) 44–53.

[4] G. Romanowski, Synthesis, characterization and catalytic activity in the oxidation of sulfides and styrene of vanadium(V) complexes with tridentate Schiff base ligands, J. Mol. Catal. A Chem. 368-369 (2013) 137–144.

[5] N.T. Thao, H.H. Trung, Selective oxidation of styrene over Mg–Co–Al hydrotalcite like-catalysts using air as oxidant, Catal. Commun. 45 (2014) 153–157.

[6] J. Huang, C. Liu, D. Sun, Y. Hong, M. Du, T. Odoom-Wubah, Biosynthesized gold nanoparticles supported over TS-1 toward efficient catalyst for epoxidation of styrene, Chem. Eng. J. 235 (2014) 215–223.

[7] T. Duarte, A. Estrada, M. Simões, I. Santos, A. Cavaleiro, M. Neves, J. Cavaleiro, Homogeneous catalytic oxidation of styrene and styrene derivatives with hydrogen peroxide in the presence of transition metal-substituted polyoxotungstates, Catal. Sci. Technol. 5 (2015) 351–363.

[8] A.S. Kanmani, S. Vancheesan, Oxidation of cyclohexene and styrene catalysed by ruthenium(II) complexes under homogeneous conditions, Stud. Surf. Sci. Catal. 113 (1998) 285–292.

[9] J. Liu, Z. Wang, P. Jian, R. Jian, Highly selective oxidation of styrene to benzaldehyde over a tailor-made cobalt oxide encapsulated zeolite catalyst, J. Colloid Interface Sci. 517 (2018) 144–154.

[10] F. Azzolina Jury, I. Polaert, L. Estel, L. Pierella, Synthesis and characterization of MEL and FAU zeolites doped with transition metals for their application to the fine chemistry under microwave irradiation, Appl. Catal. A Gen. 453 (2013) 92–101.

[11] J.H. Tong, X.D. Cai, H.Y. Wang, Q.P. Zhang, Improvement of catalytic activity in selective oxidation of styrene with $H_2O_2$ over spinel Mg–Cu ferrite hollow spheres in water, Mater. Res. Bull. 55 (2014) 205–211.

[12] S.K. Pardeshi, R.Y. Pawar, SrFe2O4 complex oxide an effective and environmentally benign catalyst for selective oxidation of styrene, J. Mol. Catal. A Chem. 334 (2011) 35–43.

[13] A. Bhalla, R. Guo, R. Roy, The perovskite structure – a review of its role in ceramic science and technology, Mater. Res. Innov. 4 (2000) 3–26.

[14] C.C. Hu, H. Teng, Influence of structural features on the photocatalytic activity of NaTaO3 powders from different synthesis methods, Appl. Catal. A General 331 (2007) 44–50.

[15] M. Yeh, C. Lin, C. Vu, K. Hsu, S. Lee, W. Li, C. Yen, Post-calcination effects of sodium tantalate synthesized by microwave-assisted hydrothermal method and its photocatalytic performance under UV and visible light, Mat. Res. Bull. 90 (2017) 182–187.

[16] O. Taran, A. Ayusheev, O. Ogorodnikova, I. Prosvirin, L. Isupova, V. Parmon, Perovskite-like catalysts LaBO3 (B═Cu, Fe, Mn, Co, Ni) for wet peroxide oxidation of phenol, Appl. Catal. B: Environ. 180 (2016) 86–93.

[17] M. Peña, J.L.G. Fierro, Chemical structures and performance of perovskite oxides, Chem. Rev. 101 (2001) 1981–2017.

[18] L. Huang, Q. Chan, B. Zhang, X. Wu, P. Gao, Z. Jiao, Y. Liu, Chin. J. Catal. 32 (2011) 1822–1830.

[19] J. Iranmanhboob, D. Hill, H. Toghiani, Characterization of $K_2CO_3$/CO−MoS2 catalyst by XRD, XPS, SEM, and EDS, Appl. Surf. Sci. 185 (2001) 72–78.

[20] X. Fu, X. Wang, D. Leung, W. Xue, Z. Ding, H. Huang, X. Fu, Photocatalytic reforming of glucose over La doped alkali tantalate photocatalysts for H2 production, Catal. Comm. 12 (2010) 184–187.

[21] N. Escalona, S. Fuentealba, G. Pecchi, Fischer–Tropsch synthesis over LaFe1 − xCoxO3 perovskites from a simulated biosyngas feed, Appl. Catal. A Gen. 381 (2010) 253–260.

[22] Z. Lu, Y. Tang, L. Chang, Y. Li, Shape-controlled synthesis and characterization of BaZrO3 microcrystals, J. Cryst. Growth 266 (2004) 539–544.

[23] B.K. Yun, Y.S. Koo, J.H. Jung, M. Song, S. Yoon, Possible role of hydroxyl group on local structure and phase transition of KNbO3 and KTaO3 nanocrystals, Physica B 405 (2010) 4866–4870.

[24] P.M. Vilarinho, N. Barroca, S. Zlotnik, P. Félix, M. Fernandes, Are lithium niobate (LiNbO3) and lithium tantalate (LiTaO3) ferroelectrics bioactive? Mat. Sci. Eng. C 39 (2014) 395–402.

[25] R. Shan, J. Shi, B. Yan, G. Chen, J. Yao, C. Liu, Transesterification of palm oil to fatty acids methyl ester using K2CO3/palygorskite catalyst, Energy Convers. Manag. 116 (2016) 142–149.

[26] M. Marchelek, B. Bajorowicz, P. Mazierski, A. Cybula, T. Klimczuk, M. Winiarski, N. Fijałkowska, A. Zaleska, KTaO3-based nanocomposites for air treatment, Catal. Today 252 (2014) 47–53.

[27] T. Ozawa, Critical investigation of methods for kinetics analysis of thermoanalytical data, J. Therm. Anal. 7 (1975) 601–617.

[28] K. Yang, Y. Zhang, Y. Li, P. Huang, X. Chen, W. Dai, X. Fu, Insight into the function of alkaline earth metal oxides as electron promoters for au/TiO2 catalysts used in CO oxidation, Appl. Catal B 183 (2016) 206–215.

[29] R. Watanabe, Y. Saito, C. Fukuhara, Dehydrogenation of ethylbenzene over zirconium-based perovskite-type catalysts of AZrO3 (A: Ca, Sr, Ba), Appl. Catal. A Gen. 482 (2014) 344–351.

[30] M. Alifanti, J. Kirchnerova, B. Delmon, Effect of substitution by cerium on the activity of $LaMnO_3$ perovskite in methane combustion, Appl. Catal. A Gen. 245 (2003) 231–244.

[31] E. Grabowska, Selected perovskite oxides: Characterization, preparation and photocatalytic properties—a review, Appl. Catal. B Environ. 186 (2016) 97–126.

[32] J. Tang, J. Wang, Catalytic steam gasification of coal char with alkali carbonates: a study on their synergic effects with calcium hydroxide, Fuel Process. Technol. 142 (2016) 34–41.

[33] L.B. Pierella, C. Saux, S.C. Caglieri, H.R. Bertorello, P.G. Bercoff, Catalytic activity and magnetic properties of Co–ZSM-5 zeolites prepared by different methods, Appl. Catal. A Gen. 347 (2008) 55–61.

[34] C. Saux, L. Pierella, Studies on styrene selective oxidation to benzaldehyde catalyzed by Cr-ZSM-5: Reaction parameters effects and kinetics, Appl. Catal. A Gen. 400 (2011) 117–121.

[35] J. Tong, W. Li, H. Wang, Y. Hu, Z. Zhang, A. Mahboob, Selective oxidation of styrene catalyzed by cerium-doped cobalt ferrite nanocrystals with greatly enhanced catalytic performance, J. Catal. 344 (2016) 474–481.